JOURNAL OF GUIDANCE, CONTROL, AND DYNAMICS
Vol. 19, No. 5, September–October 1996

Control and Flight Performance of Tethered Satellite Small Expendable Deployment System-II

E. C. Lorenzini* and S. B. Bortolami†
Harvard–Smithsonian Center for Astrophysics, Cambridge, Massachusetts 02138
C. C. Rupp‡
NASA Marshall Space Flight Center, Huntsville, Alabama 35812
and
F. Angrilli§
University of Padua, 35100 Padua, Italy

The second mission of the small expendable deployment system (SEDS-II) followed the successful mission of SEDS-I, which deployed freely a small instrumented probe on a 20-km tether. Unlike SEDS-I, the deployment of SEDS-II was controlled to provide a small libration amplitude and tether velocity at the end of deployment. The preflight goal for SEDS-II was a maximum libration of less than 10 deg and a final velocity of less than 1 m/s. The control problem was made difficult by the limited capabilities of the SEDS sensors and onboard computer and the large uncertainties inherent in the response of the actuator (brake) and the plant (deployer). The nonlinear, nonautonomous control problem is divided in two parts by using a numerically formulated feedback linearization, i.e., by devising 1) a nonlinear control (reference) trajectory and 2) a linear control about the reference trajectory. An ad hoc feedback law that forces the perturbed system to follow the reference trajectory is derived by using a linearized variational model. The controller is then tested, through computer simulations, for large deviations of the model parameters on the nonlinear model. The relevant flight data are also presented and compared to the reference values to demonstrate the validity and robustness of the control law, which provided a maximum libration amplitude of less than 4 deg and a final tether velocity of less than 0.02 m/s.

I. Introduction

THE small expendable deployment system (SEDS) is a lightweight hardware for deploying instrumented probes on a long tether from an orbiting vehicle.[1] During its first two flights (SEDS-I in March 1993 and SEDS-II in March 1994) a 26-kg instrumented probe was deployed to a distance of 20 km from the second stage of a Delta II rocket while in orbit around the Earth.

The main mechanical difference between the SEDS deployer and the better-known Tethered Satellite System deployer is that the former is a passive deployer that can only reel-out the tether, whereas the latter is an active deployer that can reel the tether in and out. Consequently, the mechanical simplicity of the SEDS deployer implies a greater difficulty in controlling the position of the satellite at the tether tip.

The technique adopted in active deployers for damping the tether librations after deployment by means of a yo-yo cycle[2] (i.e., by tuning the tether longitudinal motion to the libration frequency) is not possible with a passive deployer like SEDS. The strong nonlinearities of the system response also rule out the direct application of linear optimal control[3] to controlling SEDS deployment. Even the combination of feedback linearization and linear optimal control is not applicable to SEDS because the full-state vector is not available to the controller and an observer is computationally too demanding for the SEDS onboard computer (for a complete review of deployment control laws for tethered systems up to 1986, see Ref. 4). Since 1986, new control laws have been proposed for deployment of tethered systems such as those based on the minimization of the mission function.[5] These laws are not restricted to the linear case but they do require the knowledge of the full-state vector. Moreover, the present formulation of these mission-function laws[5] assumes the tether tension as the control variable; in SEDS, however, this is not a viable control variable because of the unsatisfactory accuracy of the deployer's tensiometer. In conclusion, a new and specialized control law had to be developed for controlling the deployment of SEDS-II.

SEDS-I adopted an open-loop control law[6] to slow down the tether exit velocity by activating the brake during the deployment of the last kilometer of tether. This type of control law had no effect on the libration amplitude, which at the end of the SEDS-I deployment was about 57 deg. On the contrary, SEDS-II controlled the librations to less than 4 deg off the local vertical (LV) at the end of deployment as explained later on in this paper.

Small libration amplitudes are required by several applications of tethered systems such as, for instance, a tethered probe carrying atmospheric sensors for gathering atmospheric data.[7] These sensors, typically, must be aligned within a few degrees of the wind velocity vector. As a second example, a tether-mediated orbital transfer[8] not only requires an accurate final state vector at satellite release but also accurate timing. In July 1997, the satellite SEDSAT will be injected into a higher orbit from the Shuttle by using a tether librating with the largest possible amplitude and releasing the satellite when the tether crosses the local vertical. These requirements can only be met by utilizing control laws that are capable of providing an accurate final state and, in some cases, timing, and that are insensitive to noise and to the uncertainties inherent with passive deployers.

II. Hardware Description

The SEDS deployer consists of a tether spool housed in a 33 × 25 cm (diameter) cylindrical canister. The tether unwinds from the end of a stationary reel with no parts in motion within the canister other than the tether itself (see Fig. 1). While unwinding from the spool, the tether crosses two light beams, generating an electric pulse every half a turn. By comparing the subsequent crossings of the light beams it is possible to eliminate the false counts caused by multiple crossings of a single light beam associated with local tether oscillations, thereby obtaining a count of the deployed length with an

Received April 27, 1995; revision received Feb. 16, 1996; accepted for publication Feb. 21, 1996.

*Staff Scientist, Radio and Geoastronomy Division. Senior Member AIAA.
†Visiting Scientist; also Research Fellow, University of Padua, Padua, Italy.
‡Small Expendable Deployment System Program Chief Scientist, Space Science and Applications Systems Office.
§Professor, Department of Mechanical Engineering.

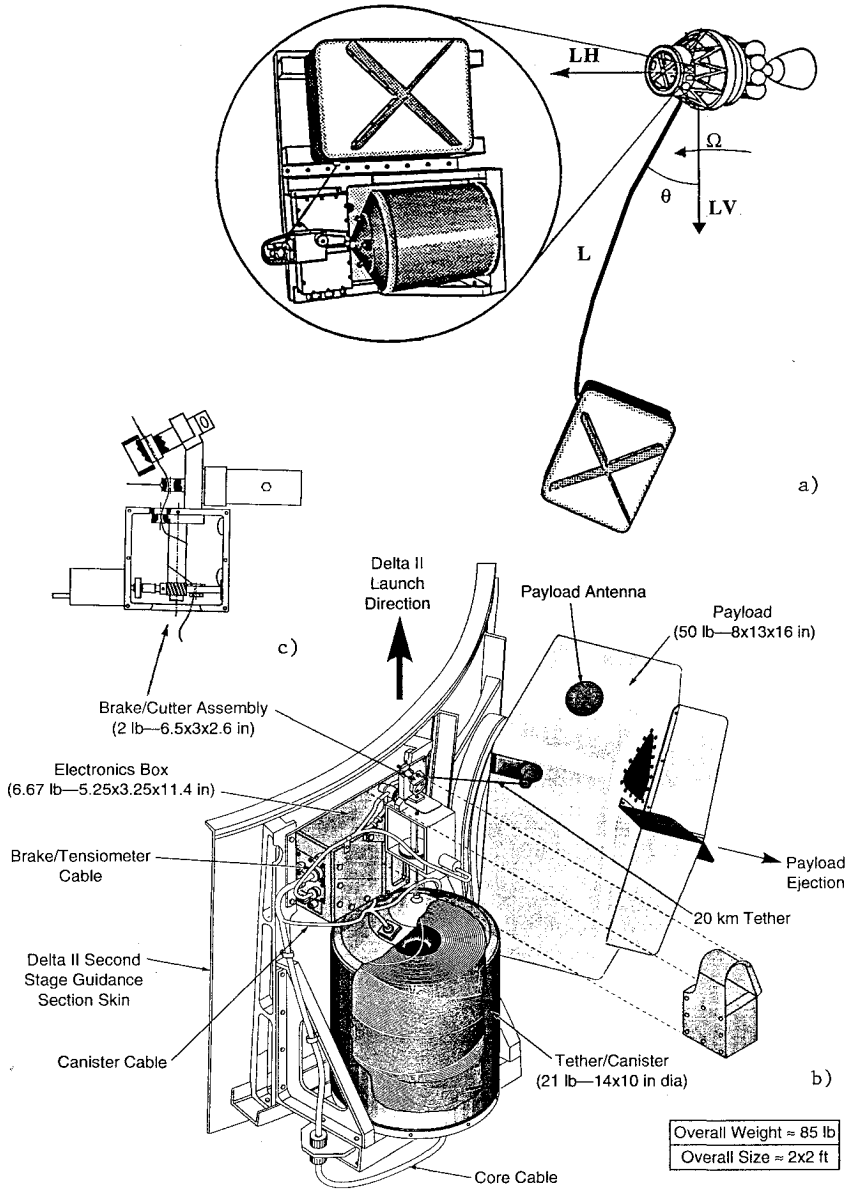

Fig. 1 Delta second stage and SEDS (courtesy of NASA and McDonnell Douglas): a) SEDS system, b) SEDS deployer and its payload on Delta's second stage, and c) enlargement of brake/cutter assembly.

accuracy of one turn (i.e., approximately 40 cm of tether length). The tether velocity can only be obtained by numerical derivation after numerical filtering for removing the high-frequency noise from the turn counters.

After exiting the canister's exit guide, the tether passes through a brake, a tensiometer, and a guillotine.[9] The tensiometer is a spring loaded device that measures the lateral pull produced by the tension, since the tether is at an angle with respect to the measuring device. The accuracy of this tensiometer is only about 10% of the full scale, and its output is very noisy because the tether fluctuates inside the guide. For this reason this tensiometer is poorly suitable as a feedback sensor in a control loop.

The brake is a barber pole activated by a stepper motor (see Fig. 1c). When the gear rotates, the tether is forced to spiral around the brake axle, thereby producing a controllable frictional force. This adjustable path braking method provides a tension that varies exponentially with the number of turns wrapped around the brake axle up to the breaking strength of the tether.

The SEDS deployer has an overall mass of 13 kg, including a 7-kg, 20-km-long tether. This tether is capable of handling payloads weighing up to 1 metric ton. The payloads for SEDS-I and SEDS-II, however, had a mass of only 26 kg. A summary of the masses and dimensions of the SEDS components[10] is shown in Table 1.

Table 1 SEDS mass and size summary

Item	Mass, kg	Size, cm
Deployer canister	3	25 × 33
Tether	7	20 km × 0.75 mm
Brake/cutter	1	8 × 8 × 20
Electronics	2	8 × 13 × 25
End mass	26	20 × 30 × 40
Brackets/clamps	4	n/a
Total	43	—

The tether for the SEDS-I and SEDS-II missions had a diameter of 0.75 mm and a linear density of 0.33 kg/km. The tether material was Spectra-1000, a high-strength polyethylene synthetic fiber, which yields a breaking strength of 850 N for the SEDS-I and SEDS-II tethers.

The deployer canister was attached to the Delta second stage (see Fig. 1a) above the miniskirt in the guidance section[11] next to the engine of the third stage. Once the third stage separated from the second stage while orbiting in low Earth orbit, the satellite was ejected by a spring loaded device with an ejection velocity of 1.64 m/s.

The 20 × 30 × 40-cm satellite, attached to the tether tip, was equipped with a radar corner reflector and instrumented with a

three-axis, 10^{-6}-g-accuracy accelerometer package, a three-axis tensiometer mounted at the tether attachment point, a three-axis, 10-mG-accuracy magnetometer, and temperature sensors.[12]

III. Tension Model

The tether exit velocity in a passive deployer strongly depends on the internal friction. The deployer frictional model, developed by Carroll,[13] is based on experimental data and the classical formula for the friction of a tight rope wrapped around a cylinder. The tether pull before the brake (internal friction) is modeled as the sum of two terms: a static term (the minimum tension T_0) and a hydraulic term proportional to the tether exit velocity $\dot{L}^2$. The brake action magnifies the internal friction by an exponential function, where the exponent is proportional to the number n of turns of the brake axle times the friction coefficient f. A second magnification factor is provided by the exit angle θ between the tether and the exit guide of the deployer. The tether tension is as follows:

$$T = \left(T_0 + I\rho\dot{L}^2 A_{\text{rel}}^{-E}\right)\exp(f \cdot |\theta_0 - \theta|)\exp(B) \tag{1}$$

where $A_{\text{rel}} = 1 - A_{\text{sol}}L/L_{\text{full}}$, L the tether deployed length, L_{full} the fully deployed tether length, A_{sol} the tether annulus solidity, B the brake parameter $= 2\pi fn$, ρ the linear density of the tether, θ the in-plane libration angle, θ_0 the null-friction exit angle, I the inertia multiplier, and E the area exponent. We refer the reader to Ref. 13 for further details about the tension model.

The tension model has a large dispersion because of the uncertainty of the static tension, the friction coefficient, and the variable tether stiffness. The minimum tension typically ranges between 10 and 40 mN, whereas the friction coefficient can vary by ±30% with respect to the most likely value of 0.18 at room temperature. Given the fact that the brake response is exponential, a ±30% uncertainty of the friction coefficient implies a maximum ±400% variation of the outboard (after the brake) tether tension about the reference value. Moreover, since the brake amplifies the internal (inboard) friction by factors as high as 90 (a number that is associated with four turns of the brake axle), the impact of the uncertainties affecting the internal deployer friction (especially T_0) on the system response is dramatic.

IV. Control Law

Additional difficulties in devising a control law are related to the onboard computer (i.e., a Z-80 mother board) with limited computational speed and only 28 kbytes of memory available for the control software.

The goal of the control design is to devise a robust control for the nonlinear plant of simple implementation and capable of handling the uncertainties, which affect the plant and the actuator. The performance goal is a libration of less than 10 deg and a tether velocity of less than 1 m/s at the end of deployment for large uncertainties of the tension values. One additional mission requirement calls for the activation of the brake only after the first kilometer of tether has been deployed, because an overbraking could stop the deployment at short range when the tether tension is low.

There are no onboard sensors for measuring the in-plane (i.e., in the orbital plane) libration angle and its derivatives. Moreover, because of the limited computational capability it is impossible to implement a state observer. The system is controllable[14] and observable (results yet to be published). Consequently, the control law must be based necessarily on the measurable variables L and $\dot{L}$.

The solution to the control problem was found by utilizing a numerically formulated feedback linearization technique.[15] Specifically, the derivation of the control law requires 1) solving a two-point boundary value problem for obtaining the nonlinear portion of the control law and 2) the implementation of a local linear-feedback regulator for a linear-time-varying (LTV) system. The solution of the boundary value problem, by means of a numerical optimization technique, provides the reference trajectory, i.e., the reference control input $\bar{B}$ (brake profile vs time) that steers the system along the desired status $\bar{L}$ (reference length) and $\dot{\bar{L}}$ (reference velocity) under nominal conditions, namely, in the absence of external disturbances and for nominal response of the actuator and the plant. The local feedback regulator corrects the reference brake profile based on the length and velocity error signals with respect to the reference length and velocity profiles when disturbances or uncertainties are present.

Two-Point Boundary Value Problem

The synthesis of the reference brake profile $\bar{B}$ is based on the search for a time function $B(t)$ that provides a solution to the deployment equations with the desired initial and final state vectors. A local vertical/local horizontal (LV-LH) reference frame is adopted with the Z axis along the nadir and the X axis pointing toward the flight velocity vector. The deployment equations of SEDS in the hypothesis of planar motion (in the orbital plane) and circular orbit are as follows:

$$\ddot{\theta} + 2(\dot{L}/L)(\dot{\theta} - \Omega) + (3/2)\Omega^2 \sin(2\theta) = 0 \tag{2a}$$

$$\ddot{L} - L\{(\dot{\theta} - \Omega)^2 + \Omega^2[3\cos^2(\theta) - 1]\} = -(1/m)\left(\tau_1 \cdot T_0 + \tau_2 \cdot I\rho\dot{L}^2 A_{\text{rel}}^{-E}\right)\exp(B + f \cdot |\theta_0 - \theta|) \tag{2b}$$

where $A_{\text{rel}} = 1 - A_{\text{sol}}L/L_{\text{full}}$ and τ_1 and τ_2 are uncertainty coefficients that are equal to unity for reference conditions.

For numerical purposes, the deployment time was divided into $k-1$ time intervals bounded by $i = 1, \ldots, k$ switch points. Values of time and controlled brake turns (t_i, B_i) are associated to each ith switch point. The function $B(t)$ is, then, approximated by means of a k-segment, piecewise function. In this particular problem k cubic splines were adopted to approximate $B(t)$. These cubic splines are identified by the set of coordinates of the switch points (t_i, B_i), $i = 1, \ldots, k$. After assuming a set of switch times t_i, a set of functions $B(t)$ can be obtained by varying the choice of the switch values $(B_1, \ldots, B_k) \in R^k$. Since the conditions for the uniqueness of the solution are valid, it is possible to obtain a set of different solutions (or equivalently deployments trajectories) of the deployment equations that satisfy the boundary conditions and depend on k parameters. The most suitable deployment trajectory, i.e., the solution that reaches the deployed position with the desired final state $(L_{\text{goal}}, \dot{L}_{\text{goal}}, \theta_{\text{goal}}, \dot{\theta}_{\text{goal}})$, is selected from this set.

Because SEDS-II should be ideally motionless with respect to LV at the end of deployment, an appropriate final state is $L_{\text{goal}} = 20{,}000$ m, $\dot{L}_{\text{goal}} = 0.1$ ms^{-1}, $\theta_{\text{goal}} = 0$, and $\dot{\theta}_{\text{goal}} = 0$ with respect to the LV-LH frame centered at the deployer. The nonnull (but small) final velocity was adopted to prevent a termination of the deployment before due time under actual flight conditions. The following cost function was then adopted:

$$F = C_1(L_{\text{end}} - L_{\text{goal}})^2 + C_2(\dot{L}_{\text{end}} - \dot{L}_{\text{goal}})^2 + C_3(\theta_{\text{end}} - \theta_{\text{goal}})^2 + C_4(\dot{\theta}_{\text{end}} - \dot{\theta}_{\text{goal}})^2 + G \tag{3}$$

where $(L_{\text{end}}, \dot{L}_{\text{end}}, \theta_{\text{end}}, \dot{\theta}_{\text{end}})$ is the final state of a generic trajectory, C_i, $i = 1, \ldots, 4$, are positive real constants, and G is a real and positive function. Hence, F is a positive function of the k parameters $(B_1, \ldots, B_k) \in R^k$. Consequently, if F is continuous it has at least an absolute minimum (optimal solution) in a compact domain of R^k. In summary, the optimal set of switch points $(\bar{B}_1, \ldots, \bar{B}_k)$ defines the optimal brake profile $\bar{B}(t)$ that yields the deployment trajectory with the desired final state $(L_{\text{goal}}, \dot{L}_{\text{goal}}, \theta_{\text{goal}}, \dot{\theta}_{\text{goal}})$. The continuity of the function F holds for the particular problem presented here.

The most convenient approach for computing the optimal solution is numerical. An integrator and an optimization algorithm are needed. The integrator in this specific case was a fourth-order Runge–Kutta and the optimization algorithm was a simplex method for function minimization[16] that does not need gradient information. The motion equations must be integrated every time the optimization algorithm tries new switch values (normally, 200–500 times).

The optimization routine[16] first makes a trial selection of the brake parameters B_i, $i = 1, \ldots, k$, in a bounded hypervolume of k dimensions. Subsequently, the numerical integrator is utilized to compute the final state of the system and, hence, the cost function. Based on the variational trend of the cost function from one iteration to the next, the optimization routine selects successive sets of values for the brake parameters B_i.

To warrant that all minima are found, the minimization of the function F is repeated starting from several different initial points in the domain R^k. Each initial point yields a minimum. All of the minima belong to a limited set. The trajectory in the state space most suitable for the control performance is chosen from this set. With reference to the goal stated earlier for SEDS-II, a typical final state (in Cartesian coordinates) is as follows: $Z = 19,999.9$ m, $\dot{Z} = 0.128$ ms^{-1}, $X = 0.15$ m, $\dot{X} = 0.0026$ ms^{-1}, and a deployment time of 6500 s.

The function G in the cost function has been adopted to obtain a relatively sustained deployment rate (i.e., $\dot{L} > 0.4$ ms^{-1} at short ranges). This constraint ensures that the satellite has enough kinetic energy to overcome unexpected discontinuities along the tether. G is a constraint function that penalizes the trajectories with rate values smaller than the predetermined minimal rate values. An example of the convergence process of the optimization algorithm is shown in Fig. 2.

This parametric optimization algorithm can provide reference profiles for any reasonable initial and final conditions of the state vector and reasonable control constraints other than those adopted for this particular SEDS-II mission.

LTV Model

The optimal profile $\bar{B}$ is the nominal control of the brake. It steers the system along the reference state trajectory $\bar{L}(t)$, $\dot{\bar{L}}(t)$, $\bar{\theta}(t)$, $\dot{\bar{\theta}}$ [note that $\bar{\theta}(t)$ and $\dot{\bar{\theta}}(t)$ are not feedback variables] that accomplishes the control goal under reference conditions. In an actual situation in which disturbances and uncertainties are present, a local regulator is needed to force the system to follow the reference trajectory. The regulator must increase the stability of the dynamic response and provide robustness to the control law. To investigate the system response around the reference trajectory, a linearized, variational model of the system was derived. The variational model that describes the system dynamics in the neighborhood of the reference trajectory has the general form

$$f\left(\ddot{\bar{\theta}}, \dot{\bar{\theta}}, \bar{\theta}, \ddot{\bar{L}}, \dot{\bar{L}}, \bar{L}\right) + \Delta f\left(\Delta\ddot{\theta}, \Delta\dot{\theta}, \Delta\theta, \Delta\ddot{L}, \Delta\dot{L}, \Delta L\right) = 0 \quad (4a)$$

$$g\left(\ddot{\bar{\theta}}, \dot{\bar{\theta}}, \bar{\theta}, \ddot{\bar{L}}, \dot{\bar{L}}, \bar{L}\right) + \Delta g\left(\Delta\ddot{\theta}, \Delta\dot{\theta}, \Delta\theta, \Delta\ddot{L}, \Delta\dot{L}, \Delta L\right)$$
$$= T\left(\bar{B}, \dot{\bar{L}}, \bar{L}, \bar{\tau}_1, \bar{\tau}_2\right) + \Delta T(\Delta B, \Delta\dot{L}, \Delta L, \delta\tau_1, \delta\tau_2) \quad (4b)$$

where $\bar{f} = 0$, $\bar{g} = \bar{T}$ because the reference trajectory is a solution of the nonlinear deployment equations. Moreover, we assume that the libration angle θ is always smaller than the null-friction exit angle θ_0 (i.e., $\theta_0 - \bar{\theta} > 0$ in the following equations). Consequently, the variational equations of the system become

$$\Delta\ddot{\theta} = 2\frac{\dot{\bar{L}}\left(\dot{\bar{\theta}} - \Omega\right)}{\bar{L}^2}\Delta L - 2\frac{\left(\dot{\bar{\theta}} - \Omega\right)}{\bar{L}}\Delta\dot{L} - 3\Omega^2\cos(2\bar{\theta})\Delta\theta - 2\frac{\dot{\bar{L}}}{\bar{L}}\Delta\dot{\theta} \quad (5a)$$

$$\Delta\ddot{L} = \left\{\Omega^2[3\cos^2(\bar{\theta}) - 1] + (\dot{\bar{\theta}} - \Omega)^2 - \frac{I\rho E A_{\text{sol}}\dot{\bar{L}}^2}{mL_{\text{full}}A_{\text{rel}}^{E+1}}\exp[\bar{B} + f(\theta_0 - \bar{\theta})]\right\}\Delta L - \frac{2I\rho\dot{\bar{L}}}{mA_{\text{rel}}^E} \times \exp[\bar{B} + f(\theta_0 - \bar{\theta})]\Delta\dot{L} + \left[-6\Omega^2\bar{L}\cos(\bar{\theta})\sin(\bar{\theta}) + \frac{f\bar{T}}{m}\right]\Delta\theta + 2\bar{L}(\dot{\bar{\theta}} - \Omega)\Delta\dot{\theta} - \left(\frac{\bar{T}}{m}\right)\Delta B - \left(\frac{T_0}{m}\right) \times \exp[\bar{B} + f(\theta_0 - \bar{\theta})]\delta\tau_1 - \left(\frac{I\rho\dot{\bar{L}}^2}{mA_{\text{rel}}^E}\right) \times \exp[\bar{B} + f(\theta_0 - \bar{\theta})]\delta\tau_2 \quad (5b)$$

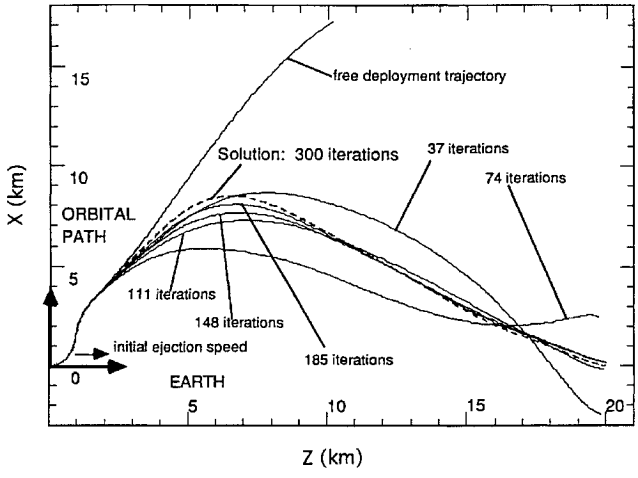

Fig. 2 Convergence process of optimization algorithm.

where

$$\bar{T} = \left[T_0 + I\rho\dot{\bar{L}}^2\bar{A}_{\text{rel}}^{-E}\right]\exp[\bar{B} + f(\theta_0 - \bar{\theta})]$$

$$\bar{A}_{\text{rel}} = \frac{1 - A_{\text{sol}}\bar{L}}{L_{\text{full}}}$$

Equations (5) can be reduced to the state–space form as follows:

$$\dot{\boldsymbol{X}} = \boldsymbol{AX} + \boldsymbol{Bu} + \boldsymbol{FW} \quad (6a)$$

$$\boldsymbol{Y} = \boldsymbol{CX} \quad (6b)$$

where

$$\boldsymbol{X} = \begin{bmatrix}\Delta L\\ \Delta\theta\\ \Delta\dot{L}\\ \Delta\dot{\theta}\end{bmatrix};\quad \boldsymbol{A} = \begin{bmatrix}0 & 0 & 1 & 0\\ 0 & 0 & 0 & 1\\ a_{31} & a_{32} & a_{33} & a_{34}\\ a_{41} & a_{42} & a_{43} & a_{44}\end{bmatrix};\quad \boldsymbol{B} = \begin{bmatrix}0\\ 0\\ b_3\\ 0\end{bmatrix}$$

$$\boldsymbol{F} = \begin{bmatrix}0 & 0\\ 0 & 0\\ f_{31} & f_{32}\\ 0 & 0\end{bmatrix};\quad \boldsymbol{W} = \begin{bmatrix}\delta\tau_1\\ \delta\tau_2\end{bmatrix};\quad \boldsymbol{C} = [0\quad 1\quad 0\quad 0] \quad (7)$$

and, consequently, $\boldsymbol{Y} = y$ (a scalar) $= \Delta\theta$.

The coefficients a_{ij}, f_{ij}, and b_3 are known functions of time as follows:

$$a_{31} = 3\Omega^2\cos^2(\bar{\theta}) + \dot{\bar{\theta}}^2 - 2\Omega\dot{\bar{\theta}} - \left[\frac{I\rho E A_{\text{sol}}\dot{\bar{L}}^2}{mL_{\text{full}}A_{\text{rel}}^{E+1}}\right]\exp[\bar{B} + f(\theta_0 - \bar{\theta})]$$
$$a_{32} = -6\Omega^2\bar{L}\cos(\bar{\theta})\sin(\bar{\theta}) + f\bar{T}/m$$
$$a_{33} = -\left[\frac{2I\rho\dot{\bar{L}}}{mA_{\text{rel}}^E}\right]\exp[\bar{B} + f(\theta_0 - \bar{\theta})];\qquad a_{34} = -2\Omega\bar{L} + 2\bar{L}\dot{\bar{\theta}} \quad (8)$$
$$a_{41} = \frac{2\dot{\bar{L}}\left(\dot{\bar{\theta}} - \Omega\right)}{\bar{L}^2};\qquad a_{42} = -3\Omega^2\cos(2\bar{\theta})$$
$$a_{43} = -\frac{2\dot{\bar{L}}\left(\dot{\bar{\theta}} - \Omega\right)}{\bar{L}};\qquad a_{44} = -\frac{2\dot{\bar{L}}}{\bar{L}}$$
$$f_{31} = -\left(T_0/m\right)\exp[\bar{B} + f(\theta_0 - \bar{\theta})]$$
$$f_{32} = -\left[\frac{I\rho\dot{\bar{L}}^2}{mA_{\text{rel}}^E}\right]\exp[\bar{B} + f(\theta_0 - \bar{\theta})];\qquad b_3 = -\frac{\bar{T}}{m}$$

In Eqs. (6), $u = \Delta B$ is the control variable and $\boldsymbol{W}$ is the vector of disturbances, i.e., in our case, the deviations from the reference

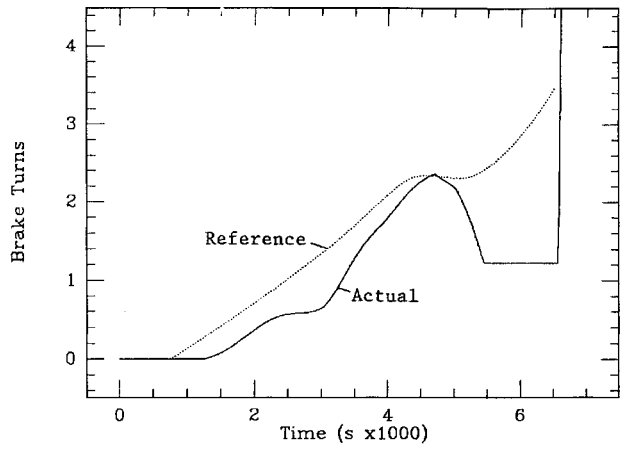

a) In-plane tether libration angle

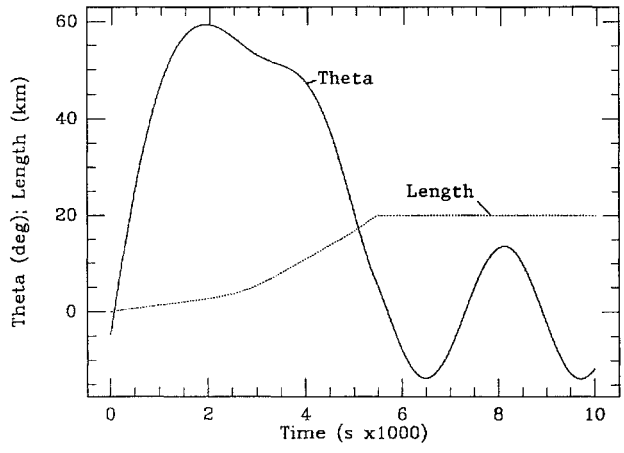

b) Brake turns

Fig. 3 Deployment dynamics for a PD controller without the reference brake profile, $B = u$ (i.e., without feedback linearization).

tension. Note also that since $\bar{T} > 0$, $b_3 < 0$. This LTV system is representative of the nonlinear system for small deviations.

In summary, the analysis of the local (about the reference trajectory) control of SEDS-II can be treated as a regulator problem for an LTV system.

Feedback Law

To prove that the feedback linearization is critical to controlling a highly nonlinear system like SEDS, Fig. 3 shows the deployment dynamics for a simulation in which a proportional-derivative (PD) regulator without the nonlinear component $\bar{B}$, i.e., $B = k_1\delta L + k_2\delta\dot{L}$, is used for forcing the nonlinear system of Eqs. (2) to track the length and speed reference profiles. In the preceding expression, B is the overall brake control and the plus signs in the control law should not come as a surprise, bearing in mind that the multiplier of the brake model in Eq. (2b) is always negative. It is evident from Fig. 3 that the system performance is unsatisfactory even for reference conditions.

It is, therefore, necessary to follow the route of feedback linearization with a feedforward component $\bar{B}$ and a linear feedback component. A fairly general formulation of the nonlinear control law would be

$$B = \bar{B} + u \tag{9a}$$

where

$$u = k_1\delta L + k_2\delta\dot{L} \tag{9b}$$

is the linear feedback, with k_1 and k_2 the control gains and δL and $\delta\dot{L}$ the length and velocity errors with respect to the reference length and velocity profiles.

At this point the problem arises of selecting suitable control gains for tracking effectively the desired trajectory in the state space by taking into account that the implementation of the control scheme must require the smallest possible computer memory.

We first analyze Eqs. (6) to gain insight into the LTV system response. After considering that a closed-loop control law for the variational system is, in general, $u = \boldsymbol{KX} = -(1/b_3)\boldsymbol{K}^*\boldsymbol{X}$, where $\boldsymbol{K} = -(1/b_3)\boldsymbol{K}^*$ is the gain matrix expressed in familiar units, Eqs. (6) yield

$$\dot{\boldsymbol{X}} = (\boldsymbol{A} - \boldsymbol{K}^*)\boldsymbol{X} + \boldsymbol{FW} \tag{10a}$$

$$y = \boldsymbol{CX} \tag{10b}$$

For our PD control law, $\boldsymbol{K} = [k_1\ 0\ k_2\ 0]$ and $\boldsymbol{K}^* = -b_3[k_1\ 0\ k_2\ 0]$.

The quasistatic transfer function of the LTV system between the input $\delta\tau_i$, $i = 1, 2$ (where $\delta\tau_1$ and $\delta\tau_2$ are the static- and hydraulic-tension errors, respectively), and the output $y = \Delta\theta$ (i.e., the libration error) is as follows[17]:

$$H_i(s) = \frac{y(s)}{w_i(s)} = \frac{\boldsymbol{CE}_1 f_{3i} s^3 + \boldsymbol{CE}_2 f_{3i} s^2 + \boldsymbol{CE}_3 f_{3i} s + \boldsymbol{CE}_4 f_{3i}}{s^4 + \chi_1 s^3 + \chi_2 s^2 + \chi_3 s + \chi_4} \qquad i = 1, 2 \tag{11}$$

where

$$\begin{aligned} \boldsymbol{A}^* &= \boldsymbol{A} - \boldsymbol{K}^*; & \boldsymbol{E}_1 &= \boldsymbol{I} \\ \chi_1 &= -\mathrm{tr}(\boldsymbol{A}^*\boldsymbol{I}); & \boldsymbol{E}_2 &= \boldsymbol{A}^*\boldsymbol{E}_1 + \chi_1\boldsymbol{I} \\ \chi_2 &= -\tfrac{1}{2}\mathrm{tr}(\boldsymbol{A}^*\boldsymbol{E}_2); & \boldsymbol{E}_3 &= \boldsymbol{A}^*\boldsymbol{E}_2 + \chi_2\boldsymbol{I} \\ \chi_3 &= -\tfrac{1}{2}\mathrm{tr}(\boldsymbol{A}^*\boldsymbol{E}_3); & \boldsymbol{E}_4 &= \boldsymbol{A}^*\boldsymbol{E}_3 + \chi_3\boldsymbol{I} \\ \chi_4 &= -\tfrac{1}{2}\mathrm{tr}(\boldsymbol{A}^*\boldsymbol{E}_4); & \boldsymbol{E}_5 &= \boldsymbol{A}^*\boldsymbol{E}_4 + \chi_4\boldsymbol{I} = 0 \end{aligned} \tag{12}$$

Thanks to the structure of the matrices $\boldsymbol{A}$, $\boldsymbol{C}$, and $\boldsymbol{K}$ in our case, the expressions of the transfer function coefficients are fairly simple:

$$\begin{aligned} \chi_1 &= -\left(a^*_{33} + a_{44}\right); & \chi_2 &= a^*_{33}a_{44} - a_{34}a_{43} - a_{31} - a_{42} \\ \chi_3 &= a^*_{31}a_{44} - a_{32}a_{43} + a^*_{33}a_{42} - a_{34}a_{41} \\ \chi_4 &= a^*_{31}a_{42} - a_{32}a_{41} \end{aligned} \tag{13}$$

where

$$a^*_{31} = a_{31} + b_3k_1; \qquad a^*_{33} = a_{33} + b_3k_2$$

and

$$\begin{aligned} \boldsymbol{CE}_1 f_{3i} &= \boldsymbol{CE}_2 f_{3i} = 0, & i &= 1, 2 \\ \boldsymbol{CE}_3 f_{3i} &= a_{43} f_{3i}, & i &= 1, 2 \\ \boldsymbol{CE}_4 f_{3i} &= a_{41} f_{3i}, & i &= 1, 2 \end{aligned} \tag{14}$$

The step response of the variational system is representative of the actual system response to a tension error because the dominant tension error is a static error (constant throughout deployment) that can be represented by a step function. From Eqs. (11–14), the response of the libration error $\Delta\theta$ in the frequency domain to a unit-step input $\delta\tau_1$ (and similarly $\delta\tau_2$) is as follows:

$$\Delta\theta_{\mathrm{step}}(s) = \frac{a_{43}\phi_i + a_{41}\phi_i/s}{s^4 + \chi_1 s^3 + \chi_2 s^2 + \chi_3 s + \chi_4}, \qquad i = 1, 2 \tag{15}$$

where

$$\phi_1 = -(T_0/m)\exp(\bar{B} + f|\theta_0 - \bar{\theta}|) \tag{16a}$$

for a static-tension error and

$$\phi_2 = -(I\rho\dot{L}^2/m)A_{\mathrm{rel}}^{-E}\exp(\bar{B} + f|\theta_0 - \bar{\theta}|) \tag{16b}$$

for a hydraulic-tension error.

Equation (15) can then be decomposed into partial fractions as follows:

$$\Delta\theta_{\text{step}}(s) = \frac{A_0}{s} + \frac{A_1}{s-e_1} + \frac{A_2}{s-e_2} + \frac{A_3}{s-e_3} + \frac{A_4}{s-e_4} \tag{17}$$

where $e_i, i = 1, \ldots, 4$, are the eigenvalues of the characteristic matrix and $A_i, i = 0, \ldots, 4$, are time-dependent coefficients as follows:

$$A_0 = \frac{a_{41}b_3}{e_1e_2e_3e_4}$$

$$A_1 = \frac{a_{41}b_3 + a_{43}b_3e_1}{e_1^4 - e_1^3(e_2+e_3+e_4) + e_1^2(e_2e_3+e_2e_4+e_3e_4) - e_1e_2e_3e_4}$$

$$A_2 = \frac{a_{41}b_3 + a_{43}b_3e_2}{e_2^4 - e_2^3(e_1+e_3+e_4) + e_2^2(e_1e_3+e_1e_4+e_3e_4) - e_1e_2e_3e_4}$$

$$A_3 = \frac{a_{41}b_3 + a_{43}b_3e_3}{e_3^4 - e_3^3(e_1+e_3+e_4) + e_3^2(e_1e_2+e_1e_4+e_2e_4) - e_1e_2e_3e_4}$$

$$A_4 = \frac{a_{41}b_3 + a_{43}b_3e_4}{e_4^4 - e_4^3(e_1+e_2+e_3) + e_4^2(e_1e_2+e_1e_3+e_2e_3) - e_1e_2e_3e_4} \tag{18}$$

where $\chi_4 = e_1e_2e_3e_4$ and also $b_3 = \phi_1 + \phi_2$.

After applying the inverse-Laplace transformation, the quasistatic response in the time domain is readily obtained as

$$\Delta\theta_{\text{step}}(t) = A_0 + A_1\exp(e_1t) + A_2\exp(e_2t) + A_3\exp(e_3t) + A_4\exp(e_4t) \tag{19}$$

We have stressed, thus far, that the equations provide the quasistatic response because, given that the system is LTV, the analysis carried out is only valid if the time variability of the system's poles is relatively small. An indicator usually adopted to show the degree of departure of the LTV dynamics from the linear time invariant dynamics is the ratio of the time rate of change of the low-frequency eigenvalue (sometimes called dominant) over its nominal value, $\dot{\omega}/\omega^2$. The eigenvalues have been computed by numerically solving the characteristic equation at successive time snapshots and Fig. 4 shows the ratio $\dot{\omega}/\omega^2$ during deployment for the open-loop system. Although the variation of this ratio is not negligible early in deployment, the quasistatic assumption can still be accepted (zero-order approximation) to simplify the controller synthesis. Since variations of $\dot{\omega}/\omega^2$ for the closed-loop system are comparable to the variations shown for the open-loop system, the analysis of the LTV system will be conducted, for simplicity, at frozen times.

However, the ensuing analysis is utilized only for obtaining the general features of the feedback control law, whereas a well-tested tethered-system dynamics simulator[18] is utilized to obtain the actual response of the nonlinear system with the complete feedback-feedforward control law of Eq. (9a).

In its simplest formulation the feedback portion of the control law of Eq. (9b) has constant gains. One disadvantage of the constant gains is that the control authority of the feedback is relatively strong

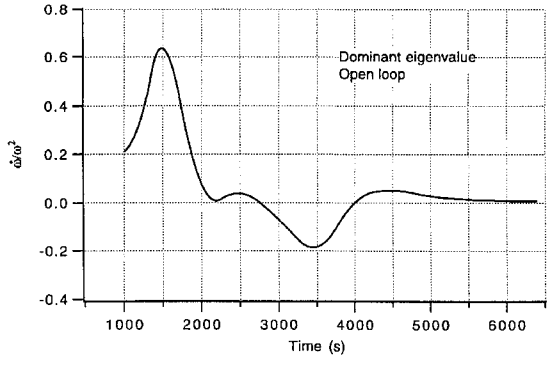

Fig. 4 Time rate of change of the low-frequency eigenvalue over its value during deployment for the open-loop LTV system.

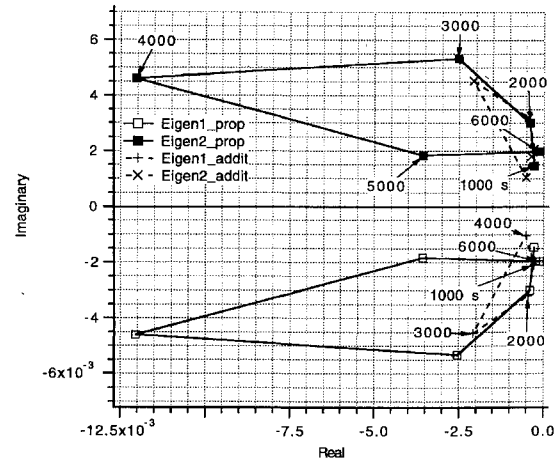

Fig. 5 Time-dependent root loci of the low-frequency eigenvalue for the additive and proportional feedback laws with gains $k_1 = 0.002$ and $k_2 = 0.2$.

for short tether lengths. Furthermore, because the control law is activated only after $t > 750$ s (i.e., for $L > 1.2$ km), the reference trajectory tracking errors may be substantial at the time of activation resulting in a sudden (and very undesirable) application of the brake at short tether length. To avoid these drawbacks, the feedback portion of the control law has been modified by weighing the control gains with the reference brake profile $\bar{B}$ as follows:

$$u = \bar{B}(k_1\delta L + k_2\delta\dot{L}) \tag{20}$$

The formulation of Eq. (20) satisfies the requirement of reducing the control authority of the feedback for short tether lengths and of enabling a gradual activation of the brake (note that $\bar{B}$ is a monotonously increasing function and that $\bar{B} = 0$ for $t \leq 750$ s). This technique of reducing the control authority was essential for being neither memory nor CPU intensive, as it uses a weighing function that is already available to the onboard computer. We will refer to the feedback law in Eq. (9b) and to the modified version of Eq. (20) as additive and proportional, respectively, because in the general formulation of the control law ($B = \bar{B} + u$) the feedback u modifies the reference brake profile $\bar{B}$ either via an additive term or via a term proportional to $\bar{B}$ itself.

Root loci have been derived for the additive and proportional control laws. These root loci are time dependent because as the time changes, the eigenvalues describe trajectories on the complex plane as a function of time. Figure 5 shows the time-dependent root-loci of the dominant eigenvalue (a pair of complex-conjugate roots) for the additive and proportional control laws for $k_1 = 0.002$ and $k_2 = 0.2$. These gains were selected on the basis of the overall dynamic response of the nonlinear plant and its actuator. Higher gains result in actuator saturations under off-nominal conditions and jittery actuator response in the presence of strong tensional noise. It is clear from the time-dependent root loci of the dominant eigenvalue that the additive and proportional control laws are quite similar in terms of frequencies of the response during deployment and that the proportional formulation has a better damping than the additive formulation during the middle of deployment.

The preceding conclusion is confirmed by the unit step response at frozen time obtained from Eq. (19). Figures 6a and 6b show the libration error $\Delta\theta$ for a unit step $\delta\tau_1$ of the static-tension error at relevant time snapshots. Note that $\delta\tau_1$ is a fractional error, i.e., $\delta\tau_1 = \Delta T_0/T_0$, where T_0 is the static tension with a reference value of 30 mN.

Figures 6a and 6b indicate, as expected, that the response of the additive feedback is prompter in the early part and more sluggish in the later part of deployment than the response of the proportional feedback law.

The final formulation of the complete feedback-feedforward brake B control law for the nonlinear system is, therefore, as follows:

$$B = \bar{B}(1 + k_1\delta L + k_2\delta\dot{L}) \tag{21}$$

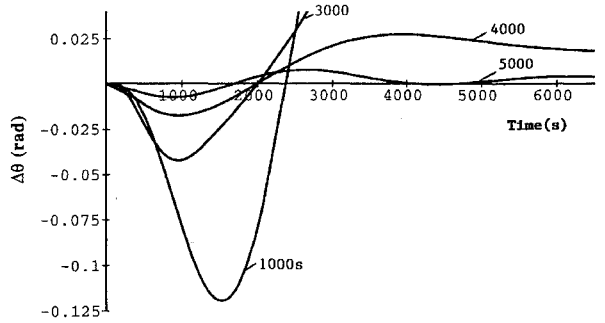

a) Additive feedback

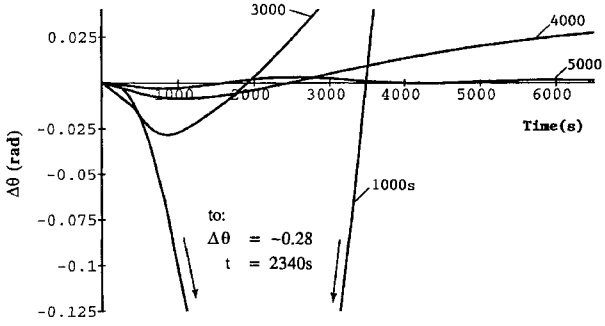

b) Proportional feedback

Fig. 6 Libration error vs time at various time snapshots for a unit step function of the static-tension error.

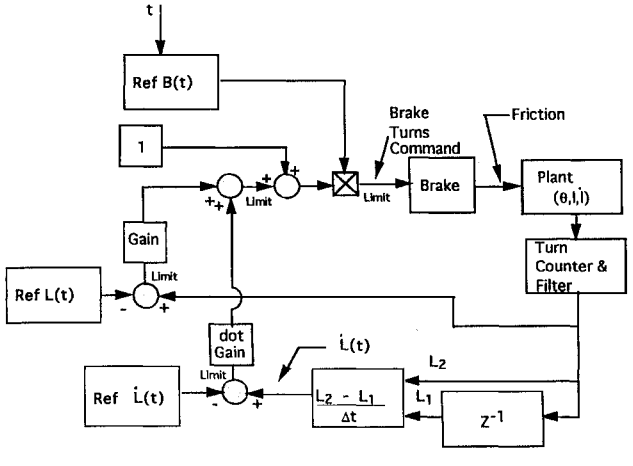

Fig. 7 Control law block diagram.

Another way of looking at this control scheme is by noting that all of the system nonlinearities are included in the reference control profile (hence the name feedback linearization), whereas the feedback provides a linear correction about the reference profile.

Brief Description of Flight Software

In the actual flight software, the reference deployed length, rate, and brake profiles are stored in the onboard computer (see Fig. 7 for the block diagram of the controller). At 1-s intervals, the output of the turn counter (proportional to the deployed tether length) is sampled and filtered by a low-pass recursive filter with a cutoff frequency of 0.02 Hz. At 8-s intervals, the actual deployment rate is computed by numerical derivation of the filtered length. The δL and $\delta \dot{L}$ error signals are computed by using the reference length and length rate profiles, and the brake is controlled according to Eq. (21). The actuation time interval of 8 s is more than adequate considering that the period of the in-plane libration is 3170 s.

Effective filtering and a suitable technique for computing the tether exit velocity from the turn counter are critical to the successful behavior of the control law. The tether, as it was observed in the SEDS-I flight data, exits the deployer in bursts and stops because its motion is dominated by a stick-slip mechanism.[6] This phenomenon results in a very noisy velocity signal if the velocity

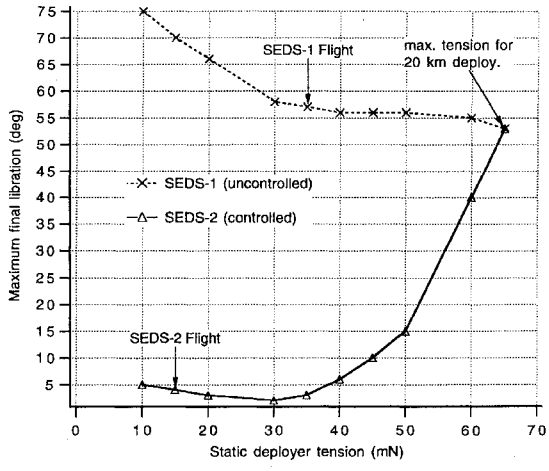

Fig. 8 Final libration amplitude vs static tether tension for the uncontrolled SEDS-I and the controlled SEDS-II.

is directly computed from the turn counter output. The technique implemented in the flight software for computing the tether exit velocity is as follows: at 1-s intervals the turn counter is sampled and filtered and the velocity is computed by numerical derivation of the filtered turn counts at 8-s intervals. This technique provides a smooth velocity signal notwithstanding the highly noisy turn counter output. A noisy velocity signal would result in an intolerably jittery response of the brake that could eventually lead to an instability.

V. Numerical Results

The center of mass of the SEDS-II system (i.e., the Delta second stage) followed a 350-km circular orbit. The satellite was ejected by means of a spring-loaded mechanism with a 1.64-m/s velocity. At $t = 750$ s (or alternatively a tether deployed length of about 1.2 km) the brake was activated and commanded by the control law.

Before discussing the flight results, we would like to discuss the robustness of the control law with respect to variations of the model parameters. The parameter in Eq. (1) with the greatest influence on the deployment dynamics is the static tension T_0. A variation of the static tension during deployment dramatically affects the tether dynamics, in general, and the tether libration, in particular. A value of $T_0 > 65$ mN stops the deployment within less than a kilometer because the initial momentum is dissipated before the gravity gradient is strong enough to overcome the frictional forces. Figure 8 shows the maximum libration amplitude vs the static tension for the uncontrolled deployment of SEDS-I and the controlled deployment of SEDS-II. These curves were obtained by means of a well-tested simulator[18] for tethered system dynamics.

It should be pointed out that the rapid decay of the performance for $T_0 > 50$ mN in Fig. 8 is not related to a lack of robustness of the control law at high values of tension. It is, instead, related to the relatively small momentum ($\dot{L}_0 = 1.64$ m/s) imparted to the satellite at ejection, which forces the control law to keep the brake fully open without exercising any control. The flight performance points for the libration-uncontrolled SEDS-I and the libration-controlled SEDS-II are shown in Fig. 8. Postflight data analysis indicates that the minimum tension was about 35 mN for SEDS-I and about 15 mN for SEDS-II. The nonlinear control law of SEDS-II was able to reduce the libration amplitude from the 57 deg of SEDS-I to less than 4 deg.

The control law is also insensitive to uncertainties in the effectiveness of the actuator. Variations as large as ±30% (or equivalently variations of ±400% of the outboard tension) with respect to the nominal value of the friction coefficient have a negligible effect on the final libration amplitude.

VI. Flight Performance

SEDS-II was a demonstration mission for testing: the controllability of deployment of tethered satellites by means of a simple, passive deployer; the long-term dynamics of an orbital tethered system; and the survivability of long tethers to micrometeoroid impacts. To this

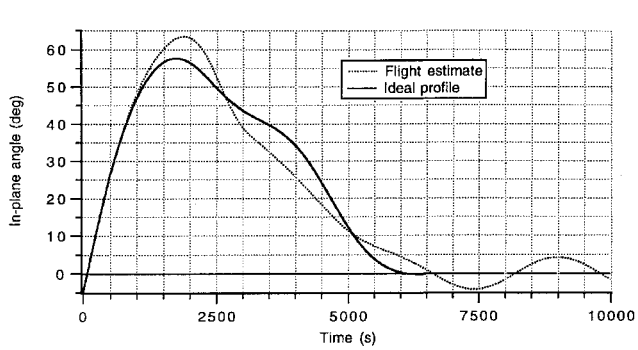

a) Tether in-plane libration with respect to local vertical

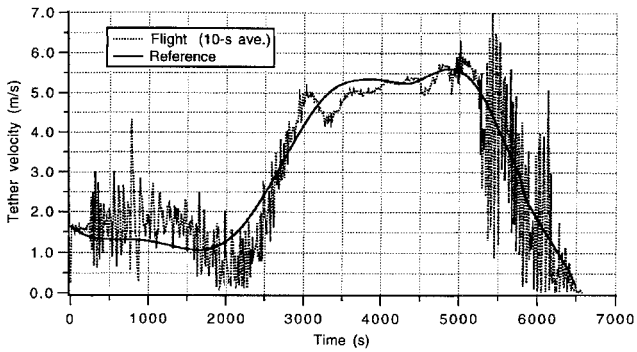

c) Tether speed (10-s average)

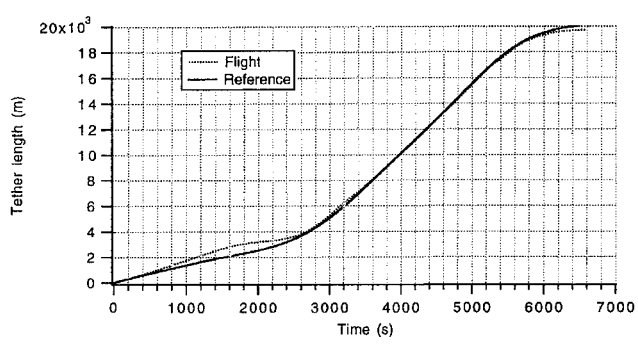

b) Tether length

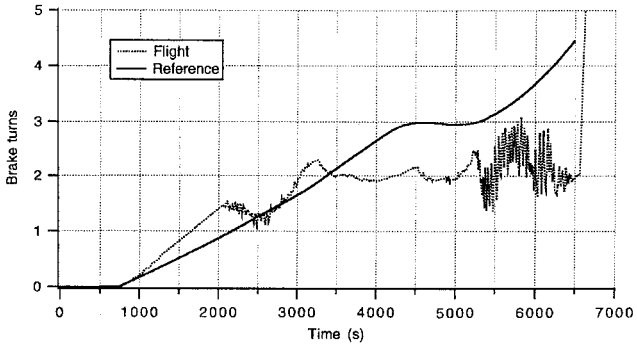

d) Brake turns

Fig. 9 Dynamic response vs time of SEDS-II during deployment.

end, unlike SEDS-I, the tether was not cut at the end of SEDS-II deployment but rather remained attached to the Delta second stage until the second stage re-entered the atmosphere two months after the launch. During that time the tethered system was intermittently tracked from ground radars, which provided the final confirmation of the libration amplitude.[19]

The estimate of the maximum tether libration was carried out by indirect methods because the libration was not measured by onboard sensors. The final libration amplitude was computed by feeding the tether-dynamics simulator with the length and velocity profiles from the flight data. This method is accurate for orbital altitudes where the influence of atmospheric drag is negligible as it is the case for SEDS-II. Figure 9a shows the estimated libration angle during the flight. This libration angle θ shown here is the component of the angle between the tether and LV in the orbital plane (in-plane for short). The component in the transverse plane (not shown here) is much smaller than the in-plane component. The ideal profile of the in-plane libration is also shown in Fig. 9a. It is called ideal as opposed to reference to alert the reader to the fact that the libration is not part of the control system, as explained before. A controller that includes the libration angle would be far more effective at tracking the desired trajectory in the state space than the control law presented here.

These libration amplitude estimates were validated by the observations with ground radars of the tethered system. The interpolation of the intermittent radar data also indicates a maximum libration amplitude of about 4 deg (Ref. 19).

Figures 9b and 9c depict, respectively, the tether length and speed vs time. The actual flight curves (dashed lines) are compared to the reference profiles (solid lines) in these figures. It must be pointed out that the reference profiles were derived for a minimum tether tension of 30 mN, which was consistent with the flight data of SEDS-I. Since the actual minimum tension for SEDS-II was about 15 mN, there is a noticeable divergence between the flight curves and the reference profiles, especially at the beginning of deployment when the control law is inactive. The ability to compensate for a value of T_0 well off-nominal is a testament to the excellent performance of the control law.

The brake actuation (see Fig. 9d) was not jittery for most of the deployment, notwithstanding the high noise level inherent in the SEDS deployer. The deployment was sufficiently smooth to provide a gentle ride for the satellite without any loss of tether tension. The more jagged behavior of the brake for $t > 5300$ s can be attributed to the multiple sling/scrub transitions that occur when the diameter of the tether spool becomes small (i.e., at the end of deployment and for small velocities, the tether starts scrubbing on the aluminum flange at the top of the deployer, see Fig. 1, with a consequent steep increase of the friction) and to the change in the winding pattern of the tether spool. The successful performance of SEDS-II during deployment proved that the control law was indeed insensitive to the noise and the uncertainties inherent in this passive deployer.

VII. Conclusions

The (closed-loop) control law of SEDS-II was developed for reducing the final libration amplitude to less than 10 deg, as opposed to the 57-deg libration amplitude exhibited by the uncontrolled SEDS-I during its flight.

The control law was insensitive to variations of the model parameters of the deployer (plant) and brake (actuator). Specifically, a variation of the most influential parameter, the static tension, between 10 and 40 mN was estimated to cause a final libration amplitude ranging from 2 to 5 deg. The control law was insensitive to large variations of the friction coefficient, which dramatically affects the brake response, and the flight data confirmed this prediction.

During the flight, the control law of SEDS-II performed as expected. The final deployment length of about 20 km was reached at $t = 6560$ s, with a final deployment speed of 0.018 m/s. The estimated maximum libration amplitude at the end of deployment was confirmed (by ground radar observations) to be 4 deg with respect to the local vertical. All of the success criteria established before the flight were met with ample margin. The control law performed in accordance with all of the preflight predictions.

The same control scheme with a different reference profile can be utilized to deploy other tethered payloads that require accurate values of the state vector at the end of deployment.

Acknowledgments

Support for this research was provided by the NASA Marshall Space Flight Center under Contract NAS8-36606. Support for Simone Bortolami while visiting the Smithsonian Astrophysical Observatory (SAO) was provided by the University of Padua and

the Radio and Geoastronomy Division of SAO. We would also like to thank James Harrison and Keith Mowery of the NASA Marshall Space Flight Center and Marco Quadrelli of the Georgia Institute of Technology for their helpful advice.

References

[1]Carroll, A. J., "The Small Expendable Deployment System (SEDS)," *Space Tethers for Science in the Space Station Era*, edited by L. Guerriero and I. Bekey, Vol. 14, Conf. Proceedings, Societá Italiana di Fisica, Bologna, Italy, 1988, pp. 43–50.

[2]Rupp, C. C., "A Tether Tension Control Law for Tethered Satellites Deployed Along Local Vertical," NASA TMX-64963, Sept. 1975.

[3]Bainum, P. M., and Kumar, V. K., "Optimal Control of the Shuttle-Tethered-Subsatellite System," *Acta Astronautica*, Vol. 7, No. 12, 1980, pp. 1333–1348.

[4]Misra, A. K., and Modi, V. J., "A Survey on the Dynamics and Control of Tethered Satellite Systems," *Tethers in Space, Advances in the Astronautical Sciences*, Vol. 62, American Astronomical Society, Univelt, San Diego, CA, 1986, pp. 667–719.

[5]Fuji, H., and Ishijima, S., "Mission Function Control for Deployment and Retrieval of a Subsatellite," *Journal of Guidance, Control, and Dynamics*, Vol. 12, No. 2, 1989, pp. 243–247.

[6]Carroll, A. J., "SEDS Deployer Design and Flight Performance," AIAA Paper 93-4764, Sept. 1993.

[7]Utah State Univ. Team, "The Tethered Satellite System Facility Requirement Definition Team," Final Rept. to NASA Marshall Space Flight Center, Contract NAS8-33383, Utah State Univ., Logan, Utah, April 1980.

[8]Henley, M. W., "Tethered OTV Operations," *Applications of Tethers in Space*, Vol. 2, NASA CP 2422, 1986, pp. 31–45.

[9]Harrison, K. J., Rupp, C. C., Carroll, J. A., Alexander, C. M., and Pulliam, E. R., "Small Expendable—Tether Deployment System (SEDS) Development Status," *Tethers in Space–Toward Flight*, AIAA, Washington, DC, 1989, pp. 19–26.

[10]Lorenzini, E. C., and Carroll, J. A., "In-Orbit Experimentation with the Small Expendable-Tether Deployment System," *ESA Journal*, Vol. 15, No. 1, 1991, pp. 27–33.

[11]Garvey, J. M., and Marin, D. R., "Delta II Secondary Payload Opportunities for Tether Demonstration Experiments," *Tethers in Space—Toward Flight*, AIAA, Washington, DC, 1989, pp. 27–32.

[12]DeLoach, R., Diamond, J., Finley, T., and Rhew, R., "End-Mass Instrumentation for the First SEDS/Delta-II Mission," AIAA Paper 90-0537, Jan. 1990.

[13]Carroll, J. A., "Users Guide to SEDS, The Small Expendable-Tether Deployment System," Tether Applications, La Jolla, CA, 1990.

[14]Bortolami, S. B., Lorenzini, E. C., Rupp, C. C., and Angrilli, F., "Control Law for the Deployment of SEDS-II," *Astrodynamics 1993*, Vol. 85, Advances in the Astronautical Sciences, 1993, pp. 733–748.

[15]Slotine, J.-J. E., and Li, W., *Applied Nonlinear Control*, Prentice–Hall, Englewood Cliffs, NJ, 1991, pp. 207–220.

[16]Nelder, J. A., and Mead, R., "A Simplex Method for Function Minimization," *Computer Journal*, Vol. 7, No. 4, 1965, pp. 308–313.

[17]Friedland, B., *Control System Design*, McGraw–Hill, New York, 1986, pp. 71–73.

[18]Lorenzini, E. C., Cosmo, M., Vetrella, S., and Moccia, A., "Dynamics and Control of the Tether Elevator/Crawler System," *Journal of Guidance, Control, and Dynamics*, Vol. 12, No. 3, 1989, pp. 404–411.

[19]Settecerri, T. J., and Stanley, J. F., "Radar and Optical Ground Measurements Final Report Small Expendable Deployer System-2," NASA Johnson Space Flight Center, Aug. 1994.